

Annual Review of Biophysics
Nonequilibrium
Thermodynamics in Cell
Biology: Extending
Equilibrium Formalism to
Cover Living Systems

Xiaona Fang¹ and Jin Wang^{1,2}

¹Department of Chemistry, Stony Brook University, Stony Brook, New York 11794, USA;
email: jin.wang.1@stonybrook.edu

²Department of Physics and Astronomy, Stony Brook University, Stony Brook, New York 11794,
USA

Annu. Rev. Biophys. 2020. 49:227–46

The *Annual Review of Biophysics* is online at
biophys.annualreviews.org

<https://doi.org/10.1146/annurev-biophys-121219-081656>

Copyright © 2020 by Annual Reviews.
All rights reserved

Keywords

nonequilibrium landscape, nonequilibrium flux, entropy production, chemical potential, heat dissipation, energy cost

Abstract

We discuss new developments in the nonequilibrium dynamics and thermodynamics of living systems, giving a few examples to demonstrate the importance of nonequilibrium thermodynamics for understanding biological dynamics and functions. We study single-molecule enzyme dynamics, in which the nonequilibrium thermodynamic and dynamic driving forces of chemical potential and flux are crucial for the emergence of non-Michaelis-Menten kinetics. We explore single-gene expression dynamics, in which nonequilibrium dissipation can suppress fluctuations. We investigate the cell cycle and identify the nutrition supply as the energy input that sustains the stability, speed, and coherence of cell cycle oscillation, from which the different vital phases of the cell cycle emerge. We examine neural decision-making processes and find the trade-offs among speed, accuracy, and thermodynamic costs that are important for neural function. Lastly, we consider the thermodynamic cost for specificity in cellular signaling and adaptation.

ANNUAL
REVIEWS **CONNECT**

www.annualreviews.org

- Download figures
- Navigate cited references
- Keyword search
- Explore related articles
- Share via email or social media

Contents

1. INTRODUCTION TO NONEQUILIBRIUM DYNAMICS AND THERMODYNAMICS	228
1.1. Global Nonequilibrium Dynamics Are Determined by Landscape and Flux ..	228
1.2. Global Nonequilibrium Thermodynamics Determined by Flux and Their Associated Entropy Production Rate	230
2. NONEQUILIBRIUM DYNAMICS AND THERMODYNAMICS FOR BIOLOGICAL PROCESSES	231
2.1. Nonequilibrium Dynamics and Thermodynamics of a Chemical Kinetic Cycle	231
2.2. Nonequilibrium Single-Molecule Enzyme Dynamics	233
2.3. The Nonequilibrium Single-Gene Expression Dynamics of Self-Regulating Systems	235
2.4. Nonequilibrium Dynamics and Thermodynamics of the Cell Cycle	236
2.5. Trade-Offs Among Accuracy, Speed, and Dissipation in Neural Decision Making	237
2.6. Energy Cost for Fidelity, Specificity, Cooperativity, and Sensitivity in Biosynthesis, Cell Signaling, and Immunity	240
2.7. Energy Cost in Cell Sensing	241
2.8. Thermodynamic Cost in Cell Adaptation	241

1. INTRODUCTION TO NONEQUILIBRIUM DYNAMICS AND THERMODYNAMICS

Cell dynamics and functions are controlled by networks full of interacting molecules and the chemical reactions among them (17). In addition, without a nutrition supply, a cell cannot function properly (3, 17). Therefore, a cell is not an isolated system. A cell is a nonequilibrium open system with the exchange of energy, information, and material with the environment. Therefore, it is crucial to quantify the dynamics and nonequilibrium thermodynamics of the cell to understand the mechanisms underlying cell functions. To quantify the nonequilibrium dynamics of the cell, one needs to identify the forces that drive them.

1.1. Global Nonequilibrium Dynamics Are Determined by Landscape and Flux

While cellular functions are regulated by the underlying gene networks (17), spatial organization and input from other cells and the environment are also important in determining a cell's function. Presently, more and more experimental studies (including high-throughput measurements) are being carried out on gene expressions, providing information on the dynamics of the underlying gene networks. One can use the information on gene expressions as a first step in characterizing the state of the cell (17). A future step will be to incorporate input from spatial organization and interactions with other cells and environments.

The expression dynamics of the gene regulatory networks can be modeled as (5)

$$\frac{d\vec{C}}{dt} = \vec{F}(\vec{C}). \quad 1.$$

In this case, $\vec{C} = \{C_1, C_2, C_3, \dots, C_n\}$ represents the expression levels of the 1, 2, 3, ..., n th genes, and $\vec{F}(\vec{C}) = \{F_1(\vec{C}), F_2(\vec{C}), F_3(\vec{C}), \dots, F_n(\vec{C})\}$ represents the driving force from the regulatory interactions of other components (genes) with the specific (1, 2, 3, ..., n th) genes. Thus, the change of the expression patterns is determined by the regulatory interactions. Local stability analyses can be performed around fixed points (47). However, the global stability is still challenging to address because we must consider the connections among states, which are missing from the local analyses.

In equilibrium systems, there is no net input from outside. As a result, the driving force and, therefore, the associated dynamics can be determined by the gradient of the interaction potential, which is associated with the equilibrium probability through the Boltzmann law (77). The equilibrium probability provides a global quantification in terms of the potential landscape through the weight of each state, from which one can establish the connections between the states. The global behavior can thus be quantified by the associated dynamics and thermodynamics (77).

In nonequilibrium systems, the global behavior cannot be addressed directly by using the equilibrium approach (47, 88). To resolve this, one can explore a stochastic version of the deterministic Equation 1. In realistic stochastic systems, intrinsic and extrinsic fluctuations are unavoidable (84), so stochastic trajectories are not predictable. However, the corresponding probability dynamics follow a linear evolution law, and that is predictable.

The stochastic trajectory dynamics follows a Langevin equation. In a continuous representation, we have $d\mathbf{C}/dt = \mathbf{F}(\mathbf{C}) + \eta$. In this case, η represents a stochastic force with the strength of the fluctuations characterized by their auto-correlation function in time $\langle \eta(\mathbf{C}, t)\eta(\mathbf{C}, t') \rangle = 2\mathbf{D}\mathbf{D}\delta(t - t')$, where D denotes a scale factor measuring the magnitude of the fluctuations, and \mathbf{D} represents the diffusion matrix that characterizes the anisotropy of the fluctuations. The corresponding probability evolution follows a Fokker-Planck equation (88): $\partial P/\partial \mathbf{t} = -\nabla \cdot \mathbf{J}$. (\cdot denotes a vector or matrix product). The change of the local probability $P(\mathbf{C}, \mathbf{t})$ in time at any location in the state space of expressions is determined by the net flux $\mathbf{J}(\mathbf{C}, \mathbf{t})$ in or out of that region. In this case, the probability flux is determined by both deterministic and stochastic driving forces (88): $\mathbf{J} = \mathbf{F}P - D\nabla \cdot (\mathbf{D}P)$.

At long times, the system reaches steady state, and the divergence of the flux becomes zero: $\nabla \cdot \mathbf{J}_{ss} = 0$. In this case, ss represents the steady state. Nonzero and nonconstant divergent free flux has no source or sink to go into or come out from and therefore is rotational or curl, meaning that the force line is circling around. A good example of this is the magnetic field. A charged particle moving in an electric field will always go along the gradient of the electric potential because the force experienced by the charged particle from the electric field is a gradient of the corresponding electric potential. For the electric field, there is a sink or source due to the presence of electric charges for the field lines to go into or come out from. Therefore, the force lines point toward or away from the source or sink (positive or negative charge). However, the magnetic field has no sink or source to get into or come out from (divergent free flux without magnetic charges). Therefore, naturally, the force experienced by the charged particle from the magnetic field is rotational or curl. One can say that the electric field generates the gradient force, and the magnetic field generates the rotational force for the motion or dynamics of the charged particle.

The presence of the nonzero steady state flux represents a net input (output) to (from) the system and breaks the detailed balance that characterizes equilibrium conditions (94). In fact, the nonzero steady state flux can be used to quantify the degree of departure from equilibrium. The driving force for nonequilibrium systems can then be decomposed into a gradient force determined by the nonequilibrium potential U , associated to the steady state probability, $U = -\ln P_{ss}$, and a rotational force involving curl flux, $\mathbf{F} = -\mathbf{D}\mathbf{D} \cdot \nabla U + \mathbf{J}_{ss}/P_{ss} + \nabla \cdot \mathbf{D}\mathbf{D}$, up to a gradient of the diffusion coefficient (92, 94). Because U is directly associated to the P_{ss} , it provides a global quantification of the state space through the weight of each state, giving rise to the landscape

topography (basins and barriers). The nonequilibrium potential under a zero fluctuation limit becomes a Lyapunov function, which can then be used to directly quantify the global stability (92, 108). One can visualize the equilibrium dynamics under detailed balance as a charged particle moving under an electric field, while nonequilibrium dynamics under broken detailed balance can be imagined as a charged particle moving under both an electric and a magnetic field (92). The driving force decomposition for the nonequilibrium systems can also be generalized to the discrete representation (for example, numbers of molecules), in which the evolution of the gene network follows a master equation (56, 74).

1.2. Global Nonequilibrium Thermodynamics Determined by Flux and Their Associated Entropy Production Rate

We are interested in the behavior of a system that is typically composed of many components or particles. If the components or particles do not interact with each other, then each of the many system configurations has an equally small chance of appearance. However, if the particles interact with each other, then some states emerge with greater probabilities (weights), distinguishing them from the others. These observable emergent states are called collective because they result from the mutual interactions among the components. For a closed physical system, the collective nature can be described by the thermodynamics (77).

Energy is conserved according to the First Law of thermodynamics. The total entropy increases in time according to the Second Law. Can the thermodynamics apply to living systems? Living systems cannot function without net energy or material input, and therefore they are nonequilibrium systems. The thermodynamics of physical equilibrium systems are well established (77). Progress has been made toward understanding nonequilibrium thermodynamics (26, 37, 63, 64, 73, 78, 79, 81, 87). It is useful to quantify the nonequilibrium thermodynamics from the perspective of the far-from-equilibrium dynamics based on the potential landscape and flux (92, 108).

For living systems, one can search for the thermodynamic origins of the dynamics in the net flux from energy pumps (89, 92, 102, 108). For cellular processes, the energy pump is the nutrition supply or the phosphorylation and dephosphorylation reactions of adenosine triphosphate (ATP) hydrolysis (73, 89, 92, 102).

1.2.1. Entropy production rate and heat dissipation in nonequilibrium thermodynamics.

To study the nonequilibrium thermodynamics, one can first start with the definition of the entropy of the system $S = -\int P(\mathbf{C}, t) \ln P(\mathbf{C}, t) d\mathbf{C}$. The time evolution of the system entropy can then be decomposed into two parts (73, 79, 92, 108): $dS/dt = dS_i/dt - dS_e/dt$. In this case, $dS_i/dt = \int d\mathbf{C}(\mathbf{J} \cdot (DD)^{-1} \cdot \mathbf{J})/P$ represents the total entropy rate of the system and environments, which is often termed the entropy production rate (EPR). It is directly related to the nonequilibrium flux \mathbf{J} . $dS_e/dt = \int d\mathbf{C}[\mathbf{J} \cdot (DD)^{-1} \cdot \mathbf{F}']$ denotes the entropy change rate of the entropy flow from the environment. The effective force \mathbf{F}' is defined as $\mathbf{F}' = \mathbf{F} - D\nabla \cdot \mathbf{D}$. One can prove that the total entropy rate dS/dt is always larger than or equal to zero (73, 79, 92, 108). This is consistent with the Second Law of thermodynamics. However, this does not guarantee that the system entropy can always be kept positive because the environment contributes to the entropy rate. A negative system entropy change gives rise to the possibility of creating order within the cell. Therefore, living systems can be in ordered low-entropy states due to exchange with the environment.

1.2.2. Quantifying the nonequilibrium thermodynamics. The energy of the system can be defined by averaging the potential landscape U using the unit of temperature T : $\langle U \rangle = -T \int P(\mathbf{C}, t) \ln P_{ss}(\mathbf{C}, t) d\mathbf{C}$. As mentioned above, the entropy of the system is defined as

$S = - \int P(\mathbf{C}, t) \ln P(\mathbf{C}, t) d\mathbf{C}$. Therefore, the free energy can be defined as $f = U - TS = T \int P(\mathbf{C}, t) \ln [P(\mathbf{C}, t) / P_{ss}(\mathbf{C}, t)] d\mathbf{C}$. One can also study the nonequilibrium thermodynamics from the free energy change in time t , which can be decomposed to $df/dt = Q_{hk}/T - dS_t/dt$ (24, 73). Therefore, one sees that $TdS_t/dt = Q_{bk} - df/dt$, where the entropy production is defined as $dS_t/dt = \int d\mathbf{C} [\mathbf{J} \cdot (\mathbf{D}\mathbf{D})^{-1} \cdot \mathbf{J}] / P$, and the housekeeping heat is defined as $Q_{hk} = T \int \mathbf{J}_{ss} / P_{ss} \cdot 1 / (\mathbf{D}\mathbf{D}) \cdot \mathbf{J}_{ss} d\mathbf{C}$. In this case, \mathbf{J} is the flux, while \mathbf{D} is a scale factor measuring the magnitude of the fluctuations, and \mathbf{D} represents the diffusion matrix, measuring the anisotropy of the fluctuations that were defined above. T is the fictitious temperature or diffusion scale coefficient characterizing the fluctuation strength, while ss represents the steady state. There are two contributions to the total entropy production dS_t/dt . One contribution comes from df/dt , the relaxation of free energy in time. The other contribution comes from Q_{hk} , denoting the housekeeping heat for maintaining the nonequilibrium steady state, supported by the steady state flux \mathbf{J}_{ss} (24, 73). Once the probability evolution of the cellular dynamics is known by either real time traces in experiments or by simulations, one can quantify the free energy change, housekeeping heat, and entropy production.

For discrete dynamics, one can quantify the nonequilibrium dynamics by the master equation: $dP_i/dt = \sum_j T_{ij}P_j - \sum_j T_{ji}P_i$ for state i , where P_i represents the probability of state i . T_{ij} represents the transition probability from state j to state i .

The nonequilibrium thermodynamics can also be formulated (38, 56, 79, 110, 111). At steady state, since $dP_i/dt = 0$, we have $\sum_j (-T_{ij}P_i^{ss} + T_{ji}P_j^{ss}) = 0$. However, the local steady state flux itself, $F_{ij}^{ss} = -T_{ij}P_i^{ss} + T_{ji}P_j^{ss}$, is not zero when detailed balance is broken. One can define a generalized chemical potential between i and j , $A_{ij} = \ln(T_{ji}P_j)/(T_{ij}P_i)$.

There exists a mapping between chemical or biological networks and electric circuits. The flux corresponds to the current, and the chemical potential A_{ij} corresponds to the voltage in an electrical circuit. The nonequilibrium systems or the networks dissipate energy in a similar way to electric circuits (38, 56, 79, 110, 111).

The system entropy S is defined as $S = - \sum_i P_i \ln P_i$, and the EPR dS_{tot}/dt is given as (38, 56, 79, 110, 111) $dS_{tot}/dt = \sum_{ij} F_{ij}A_{ij} = \sum_{ij} (T_{ij}P_j - T_{ji}P_i) \ln [(T_{ji}P_j)/(T_{ij}P_i)]$. As seen above, the EPR is directly related to the flux. Therefore, the EPR or the dissipation can also give a measure of the degree of departure from equilibrium. The flux for characterizing the nonequilibrium part of the dynamics and the entropy production characterizing the nonequilibrium thermodynamic cost can be quantified once the underlying regulatory network is specified.

2. NONEQUILIBRIUM DYNAMICS AND THERMODYNAMICS FOR BIOLOGICAL PROCESSES

2.1. Nonequilibrium Dynamics and Thermodynamics of a Chemical Kinetic Cycle

Nonequilibrium dynamics describes the time evolution of gene expressions or protein concentrations in the cell. The nonequilibrium thermodynamics describes the global thermodynamics of the whole cell in terms of the underlying gene network. A physical and quantitative measure of the nonequilibrium thermodynamics is the EPR, which can be used to quantify the thermodynamic cost for performing biological functions. In addition to the gradient potential landscape driving force specified by the steady state probability, the steady state probability flux is a driving force for nonequilibrium gene networks. It turns out that it is also the key to determining the EPR (EPR being roughly the integration of flux squared over the state space in the continuous representation) (73, 79, 92, 108). Flux is then important in determining not only the nonequilibrium dynamics, but

also the nonequilibrium thermodynamic cost for the underlying gene network evolution. Therefore, flux is the bridge between nonequilibrium dynamics and nonequilibrium thermodynamics.

Since the flux, which characterizes the amount by which the detailed balance is broken, is associated with the net input (energy, information, or material) to the system, one can explore the thermodynamic origin (e.g., net energy input) of the flux. It can be shown that the energy pump to the system, denoted by the chemical potential difference ΔG , generates not only the deterministic chemical reaction flux, but also the probabilistic flux, in analogy to electric voltage generating electric current. Using the Schnakenberg kinetic model (89), in which all of the individual reactions are reversible (102), we have



The species B and A are kept at constant concentrations, as they are the source of energy input (79, 102) related to ATP and adenosine diphosphate concentrations, for example. The concentration ratio B/A can then be used to represent the strength of the energy pump, where A , B , X , and Y represent the concentrations of the species. The forward and backward reaction fluxes J_{j+} , J_{j-} for each reaction can be defined. The chemical potential difference can thus be defined as $\Delta G_j = k_B T \ln(J_{j+}/J_{j-})$. The total chemical potential difference becomes $\Delta G_{AB} = \sum_j \Delta G_j = k_B T \ln[k_1 k_2 k_3 B / (k_{-1} k_{-2} k_{-3} A)]$ (102).

The chemical reactions specified above can have several stable states or phases depending on the concentrations of molecular species A and B. One stable state or phase is the monostable one, in which the concentrations of both chemical species X and Y reach steady state values. This state is locally stable. In addition to this specific stable state, a limit cycle oscillation state of the X and Y species can be found; no other steady state or phase is found. Therefore, a specific stable state can only be either monostable or a state of stable limit cycle oscillations.

When the system is at a steady state, the deterministic flux reaches $J_{ss} = k_2 B - k_{-2} Y_0$. Y_0 is the steady state value of Y. The deterministic flux monotonically increases as the chemical potential ΔG (ΔG_{AB}) increases in the monostability regime. Therefore, the nonequilibrium chemical potential difference ΔG leads to a nonzero deterministic flux (102). When the energy input increases, the monostable regime becomes unstable, and a limit cycle sets in. One can explore the relationship between the steady state probabilistic flux and the deterministic flux under different chemical potential differences ΔG (ΔG_{AB}). The chemical potential difference is closely related to the concentration ratio B/A . One can see that the chemical potential difference is the main factor keeping the limit cycle going (102). In analogy to the case of voltage generating the electric current, the chemical voltage (potential) drives both the average deterministic flux and the steady state probabilistic flux. There is a strong correlation between the two fluxes with respect to the chemical potential driving force (102). These numerical results and discussions support the view that the energy pump is the origin of the nonequilibrium flux (102). From the perspective of thermodynamics, the combined effect of the chemical potential difference (voltage) and flux (current) $\Delta G \times J_{ss}$ gives rise to the entropy production or the thermodynamic cost for maintaining the stability and function of the nonequilibrium system (92, 102).

2.2. Nonequilibrium Single-Molecule Enzyme Dynamics

Recent advances in technology make it possible to study chemical reaction dynamics, including enzymatic dynamics, at the single-molecule level (59). Single-molecule measurements can reveal heterogeneity in kinetic rates that are not available from bulk measurements.

Enzymatic reactions under protein conformational fluctuations are often found to obey the classic Michaelis-Menten (MM) rate law: The inverse of the enzyme catalytic rate is linear on the inverse of the substrate concentration (21, 62). The MM form is expected to be valid as long as the detailed balance condition is preserved, with no net flux between the different conformations of the fluctuating enzymes (43, 49, 98).

Single-molecule catalysis of the oxidation of dihydrorhodamine 6G into rhodamine 6G by the enzyme horseradish peroxidase (HRP) has recently been observed at room temperature (19, 20, 39). HRP in the presence of hydrogen peroxide and a nonfluorescent substrate can turn over the substrate into a fluorescent product. The catalysis is visible by fluorescence spectroscopy. The kinetic scheme for this enzyme reaction process is shown in **Figure 1a**.

HRP has two conformations, E1 and E2. The enzyme molecule binds with substrate dihydrorhodamine 123 to form the ES complex, while ES binds with substrate H_2O_2 and returns to the original enzyme state by releasing the H_2O molecule. ES represents the complex that can be observed by the fluorescence. The single enzyme dynamics can be studied by the probability evolution of the states dictated by the master equation:

$$\frac{d}{dt}P = \begin{pmatrix} -k_1[s] - \beta & \alpha & k_{-1} + k_3[\text{H}_2\text{O}_2] \\ \beta & -k_2[s] - \alpha & k_{-2} + k_4[\text{H}_2\text{O}_2] \\ k_1[s] & k_2[s] & -k_{-1} - k_{-2} - k_3[\text{H}_2\text{O}_2] - k_4[\text{H}_2\text{O}_2] \end{pmatrix} P = AP. \quad 3.$$

In this case, P represents a vector of $[P_{E1}, P_{E2}, P_{ES}]$, while P_{E1}, P_{E2}, P_{ES} represent the probabilities of the enzyme being in the E1, E2, or ES state, respectively. A transition matrix A specifies the transition probability from one state to another. From this equation, one can derive the enzyme catalytic rate. The derivation shows that the inverse of the enzyme catalytic rate is not linear with respect to the inverse of the substrate concentrations when the detailed balance is broken and the associated flux is nonzero. In such cases, we have a non-MM catalytic rate that deviates from the conventional MM rate with its inverse linear law (43, 54). Therefore, the nonequilibrium net flux that breaks the detailed balance between conformational states is a key for determining whether the enzyme follows the MM rate law. From the experimental observations shown in **Figure 1b** (54), one can see clearly the nonlinear relationship between the inverse enzyme rate and the inverse substrate concentration. The straight lines indicate the linear behavior that would have been expected for the MM rate. This shows clearly the non-MM behavior of the enzyme reaction rate with respect to the substrate. Based on this, one can quantify the flux at different substrate concentrations, as shown in **Figure 1c**. For thermodynamic characterization, the corresponding chemical potentials can be quantified based on the correlation functions of the experimental fluorescence intensity data. The chemical potential of the chemical reaction cycle can be given as

$$\begin{aligned} \Delta\mu &= \Delta\mu_{E1-ES} + \Delta\mu_{ES-E2} + \Delta\mu_{E2-E1} \\ &= k_B T \ln \frac{A_{31} P_3^S A_{12} P_1^S A_{23} P_2^S}{A_{13} P_1^S A_{32} P_3^S A_{21} P_2^S} \\ &= k_B T \ln \frac{A_{31} A_{12} A_{23}}{A_{13} A_{32} A_{21}}. \end{aligned} \quad 4.$$

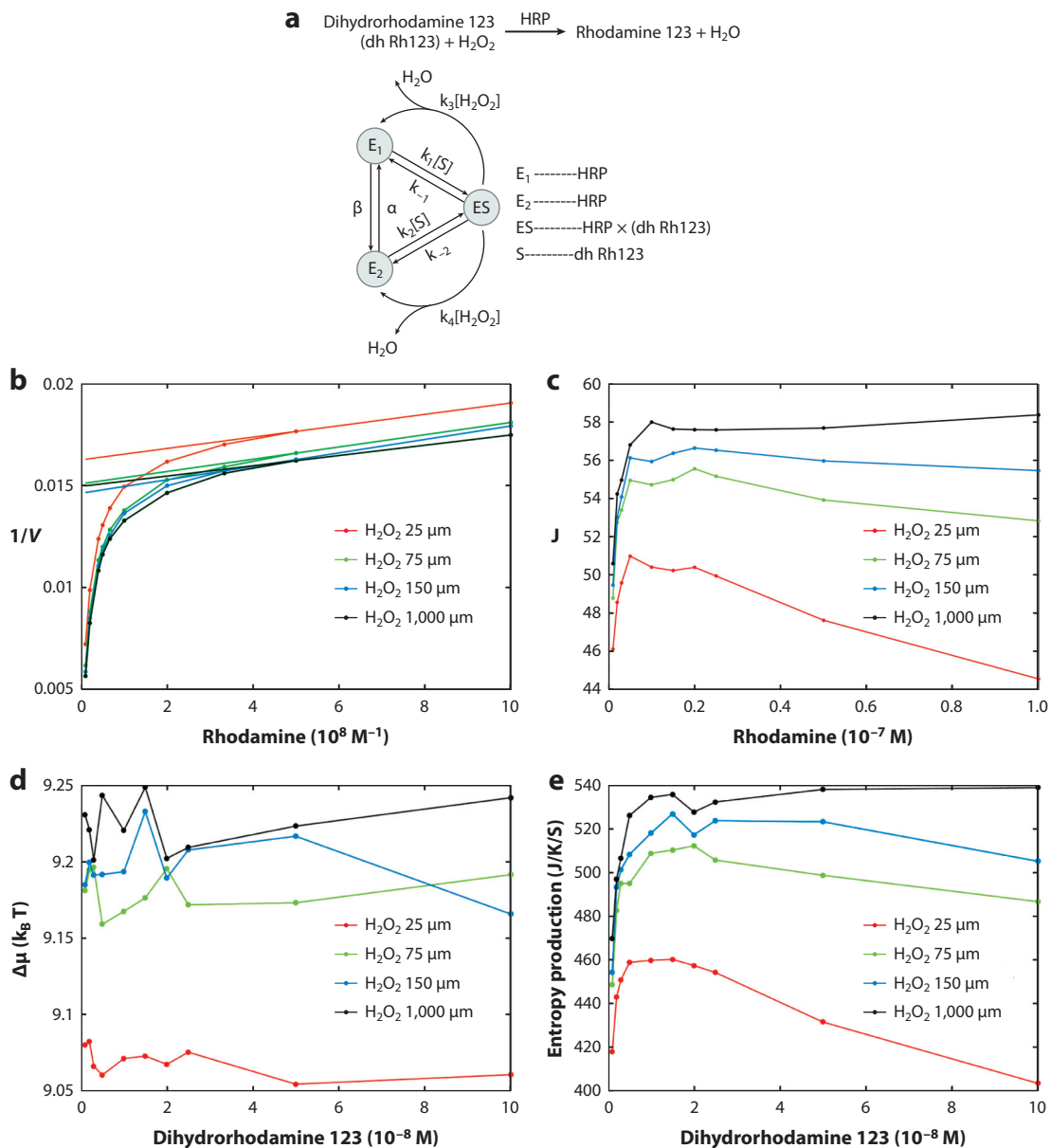


Figure 1

(a) Single-molecule enzyme reaction scheme. (b) Michaelis-Menten rates (*straight lines*) and non-Michaelis-Menten rates (*curved lines*) versus the inverse of substrate concentrations. (c) Steady state probability loop flux among the states (E1, E2, ES) versus substrate concentrations. (d) Chemical potential versus substrate concentrations. (e) Entropy production rate versus substrate concentrations. Figure adapted with permission from Reference 54. Abbreviation: HRP, horseradish peroxidase.

A_{ij} represents an element of the transition rate matrix A in the master equation. P^S represents the steady state probability. The chemical potentials at different substrate concentrations are shown in **Figure 1d** (54). The chemical potentials have almost constant values at different rhodamine substrate concentrations with certain H_2O_2 . The chemical potential thus gives rise to the energy supply sourced as a chemical battery.

The entropy production as a measure of the thermodynamic cost for maintaining the nonequilibrium steady state can also be quantified from the experimental data through correlations (54):

$$\begin{aligned} \text{EPR} &= \sum_{i,j} \left(P_i^S A_{ji} - P_j^S A_{ij} \right) \ln \frac{A_{ji} P_i^S}{A_{ij} P_j^S} \\ &= J \ln \frac{A_{31} A_{12} A_{23}}{A_{13} A_{32} A_{21}}, \end{aligned} \quad 5.$$

where the cycle flux J is given as $J = A_{12} P_{E2}^{ss} - A_{21} P_{E1}^{ss} = A_{23} P_{E3}^{ss} - A_{32} P_{E2}^{ss} = A_{31} P_{E1}^{ss} - A_{13} P_{E3}^{ss}$. The EPRs at different rhodamine substrate concentrations are shown in **Figure 1e** (54). Notice that the EPRs at different substrate concentrations have behavior similar to the flux in **Figure 1c**. This is because the flux is the origin of both the deviation from equilibrium and the entropy production.

Above, I illustrate that the nonequilibrium flux is the driving force for the non-MM behavior. The nonequilibrium flux driving the dynamics, the corresponding chemical potentials, and the associated EPR for the nonequilibrium thermodynamics can now be quantified experimentally (54). The origin of the nonequilibrium flux, the chemical potential, and the EPRs driving enzymatic reactions are identified as the energy input in the enzyme reaction through the isothermal titration calorimetry measurements of heat consumption (54).

2.3. The Nonequilibrium Single-Gene Expression Dynamics of Self-Regulating Systems

Uncovering the mechanisms of gene regulatory networks is important for understanding many cellular functions (17). To understand the network dynamics, it is essential to understand their building blocks, the network modules (17). The simplest building blocks of gene circuits are the self-regulators: self-activators and self-repressors. The corresponding gene regulation processes comprise several kinds of biochemical reactions, including binding and unbinding of regulatory proteins to the genes and syntheses and degradations of the RNAs and proteins (17).

It is often assumed that the binding and unbinding steps are much faster than the synthesis and degradation steps (adiabatic limit) (2), leading to a stable state for a self-repressor (8, 17). However, in eukaryotic cells and certain prokaryotic cells, binding and unbinding rates can be comparable to the associated synthesis and degradation rates. This can lead to naively unexpected and nontrivial stable states (6, 10, 23, 46, 50, 80).

To understand nontriviality, consider that, conventionally, one expects that a self-repressing gene can have only one state: the repressed state. However, when the proteins produced by the gene bind or unbind to repress the gene more slowly than they are synthesized (rather than more rapidly, as is conventionally expected), there is sufficient time and therefore probability for the genes to be on, and therefore a state of high expression can emerge as the result of slow binding. For some bacteria, the regulatory binding can be fast; for others, the binding can be slow. For eukaryotic cells, due to the epigenetics of histone remodeling and DNA methylation, a slower time scale sets in for regulatory binding and effectively slows it down. Therefore, we expect

the self-repressor to have this nontrivial high expression state for some bacterial cells and many eukaryotic cells. This has been tested and confirmed in experiments (14, 48, 83).

Because there are finite numbers of molecules in cells, intrinsic fluctuations in those numbers can be present. A probabilistic description based on master equations is essential for describing the underlying stochastic dynamics. From the master equations, one can derive the phase diagrams of monostability and bistability in adiabatic fast regulatory binding and nonadiabatic slow binding regimes, respectively (23). One can also explore the thermodynamic dissipation cost by calculating the EPR and correlating it with the stability through landscape topology, often measured by the barrier height and kinetics (23). Such studies provide new insights into the relationships between the stabilities of cellular states and the thermodynamic costs of maintaining those states. In a slow-binding nonadiabatic regime, the calculated EPR was seen to increase monotonically with the increase of the ratio (ω) of the regulatory binding and unbinding rates relative to the degradation rate. A higher ω implies more frequent binding and unbinding reactions between two gene states (two peaks in gene expression distributions), consuming more energy. As ω reaches the fast binding adiabatic limit, the EPR also reaches a limit and will not increase further with ω . The binding and unbinding reaches a balance such that higher ω will not consume more energy (23).

One can use the Fano factor to quantify the statistical fluctuations in terms of the ratio between the variance and mean of the gene expressions or protein concentrations. A large Fano factor implies large fluctuations in gene expression. It is interesting to see that the larger entropy production rate in the fast-binding adiabatic regime is often associated with smaller fluctuations (measured by the Fano factor); conversely, a smaller EPR in the slow-binding nonadiabatic regime is often associated with larger fluctuations (23). This indicates that there is a thermodynamic cost (the EPR) associated with the nonequilibrium dynamics (flux), which can be used for suppressing the fluctuations (23).

2.4. Nonequilibrium Dynamics and Thermodynamics of the Cell Cycle

A primary cell can have two major fates: to divide or to differentiate. The cell division or cell cycle process is crucial for growth, proliferation, and replication (12, 13, 41, 85, 86). Cell cycles go through a few phases: a resting phase called G1, a synthesis phase called S, an interphase called G2, and a mitosis phase called M. Cell cycle checkpoints are present to ensure the proper progression across each phase. The cell cycle is believed to be tightly regulated by underlying gene networks (41, 69). Significant progress has been made in describing the principles of the cell cycle. However, challenges still remain. For example, how do we understand the physical principles of the dynamics and thermodynamics for the cell cycle based on the underlying gene network? How can we identify the key elements for controlling the stability and speed of the cell cycle?

To address the dynamic and thermodynamic origins of the cell cycle, a global view based on landscape and flux theory has been suggested (52). The starting point is the mammalian cell cycle gene network (16, 28, 29). The network contains four major cyclin/Cdk complexes that dictate the cell cycle dynamics. The mutual repressions between pRB and E2F determine the cell cycle progression. At the beginning of the cell cycle, a growth factor (GF) promotes the synthesis of cyclin D and then cyclin D/Cdk4-6 (Complex 1). Activated cyclin D/Cdk4-6 and cyclin E/Cdk2 (Complex 2) can guarantee the progression of G1 and evoke the G1/S switch due to the repression of pRB. The repression of pRB leads to the activation of E2F, which generates the synthesis of G1 cyclins (Complex 2) and therefore the cell cycle progression. In the S and G2 phases (Complex 3), cyclin A/Cdk2 represses Cdh1, which induces the cyclin B degradation. The negative feedback loops from Cdc20 activation to cyclin B/Cdk1 and cyclin A/Cdk2 (Complex 4), as well as from cyclin A/Cdk2 to E2F (Complex 3), together reset the cell cycle and start a new

round of oscillations. Inhibiting phosphorylation by Wee1 and activating dephosphorylation by Cdc25 control the activity of Cdk1 and Cdk2. The dynamics of the gene regulatory network can be described by a set of nonlinear ordinary differential equations.

Both the landscape and the steady state probability flux of the cell cycle network can be quantified (52). The landscape shows an inhomogeneous irregular Mexican hat shape. From any state, the landscape attracts the cell to the oscillation ring valley. On the ring valley, it is the flux that drives the coherent oscillation of the cell cycle. Therefore, the landscape guarantees the stabilities of the states or phases of the cell cycle, while the flux guarantees the stable flow of the cell cycle (52, 92, 94). Both landscape and flux are crucial driving forces for the cell cycle dynamics. On the landscape, local basins of attraction can quantify the different cell cycle phases (G1, S/G2, M). The transition states (or barriers) between different local basins can quantify the checkpoints at different stages of the cell cycle. This gives a natural and physical description for the checkpoint mechanism of the cell cycle (52).

One can also investigate the origin of the flux as the driving force for coherent cell cycle oscillations (52). As seen in **Figure 2**, as the amount of GF increases, the nutrition supply to the cell increases, and the flux also increases. This means that the nutrition supply is the source for the emergence of the flux driving the cell cycle. This speeds up the cell cycle oscillation. However, the thermodynamic cost in terms of the EPR, which is related to the flux, also increases as the GF increases. Thus, a thermodynamic cost must be paid to maintain the coherent cell cycle oscillation. Therefore, the nutrition energy supply gives rise to both the nonequilibrium dynamic and thermodynamic forces that drive the functional oscillation of the cell cycle (52). Thus, energy input is the key to the origin of the single-cell life cycle (109).

One can also explore the relationship between the energy input in terms of the nutrition supply and the emergence of the different cell cycle phases. Without the nutrition supply, there is only one stable G1 state with a single basin of attraction. As the nutrition increases, other cell cycle states such as the S, G2, and M phases start to emerge as multiple attractors. As the nutrition supply increases even further beyond a critical point, the cell cycle Mexican hat landscape emerges (see supporting information in Reference 52). One can state that the thermodynamic energy input through the nutrition supply can alter the existing stable states and give rise to the emergence of the new states through the bifurcations or nonequilibrium phase transitions. Because the flux is rotational, it tends to destabilize the point attractors and to stabilize the line attractors as limit cycles. This can give rise to a dynamic source for the bifurcation and nonequilibrium phase transitions (for example, from point attractors to line attractors). Therefore, the flux and energy input can provide a dynamic and thermodynamic origin for the bifurcation and nonequilibrium phase transitions.

Through global sensitivity analyses of landscape topography, on the flux, and on the speeds of the cell cycle, key genes and regulators in the gene network can be identified as being crucial to the stability and function of the cell cycle (52). This can help in prediction and design of anticancer strategies.

2.5. Trade-Offs Among Accuracy, Speed, and Dissipation in Neural Decision Making

To explore how nonequilibrium dynamics and thermodynamics influence the behaviors of intercellular networks, one can study the dynamics of the neural networks that are crucial for cognitive functions such as decision making (1, 45, 53, 91). Before making an optimal decision, one often evaluates the costs and benefits, assessing the risk or uncertainty from a set of alternatives (15, 60, 66). Recently, progress has been made in both theoretical and experimental studies on

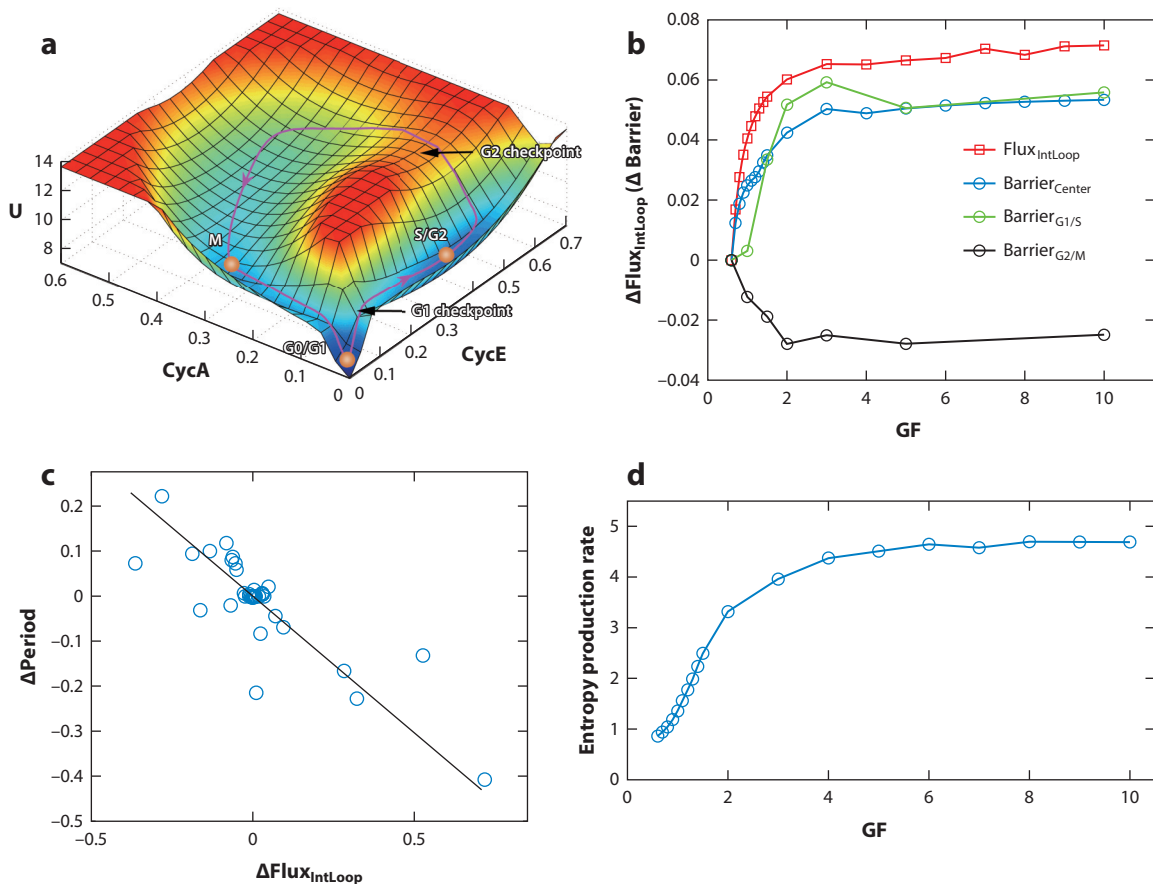


Figure 2

(a) Landscape and flux for cell cycle. The vertical axis represents U as the potential landscape, defined by the steady state probability distribution of the cell cycle network of protein concentrations or gene expressions. The purple line represents the flux force line. (b) Flux versus growth factor. (c) Period of cell cycle versus growth factor. (d) Entropy production rate versus growth factor. Figure adapted with permission from Reference 52. Abbreviation: GF, growth factor.

decision making (4, 30, 76, 97). In some of these studies, a diffusion model (75, 76) is used to help explain the behavioral data. However, the longer response times in error (wrong) decision trials compared to the response times in correct decision trails observed in experiments cannot be naturally fit by the diffusion model (82). An attractor model was suggested to explain a two-choice decision-making task (96, 100, 101) and to describe the behavioral and neurophysiological data in a decision-making process. Although the position of each attractor state can be determined, the weights of these states and the associated attractor landscape were not quantified (96, 100, 101) in the attractor model. Quantifying the topology of the attractor landscape through the weights of the states could help account for the stability of the attractors. However, understanding the interplay among the speed, accuracy, and cost, as well as the associated underlying mechanisms of the decision making, remains challenging.

From the landscape and flux theory for neural network dynamics (103–106), the basins of attraction as the fates of decision making can be identified (105). The global stability of basins of attraction can be quantified through the barrier heights and escape times from the basins (105).

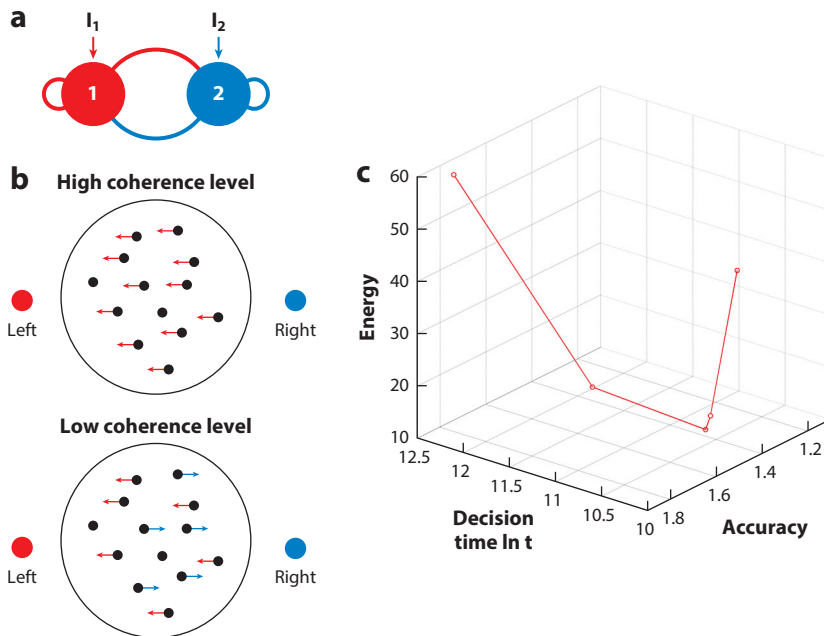


Figure 3

(a) Reduced two-population decision-making model, with two competing neural and self-promoting populations selective for leftward or rightward directions. The bars represent the repressing regulations, and the arrows represent the activating regulations. (b) Illustration of the biased dot motion under high coherence and random dot motion under low coherence. Arrows represent the direction of motion of the dots, while color represents left or right choices. (c) The trade-off among speed, accuracy, and cost. Figure adapted with permission from Reference 105.

The optimal decision-making path can also be identified (95, 105). Both the landscape and the flux dictate the dynamic processes, the decision-making speed, and the optimal path (105, 106). Moreover, the thermodynamic costs in terms of the entropy production rate related to the flux can be quantified (105). By varying stimulus input and threshold, one can quantitatively explore the underlying mechanisms of the speed–accuracy–energy trade-off (105).

Figure 3a shows a reduced two-population decision-making model for the multineuron populations, with two mutually repressing neural populations under self-activations. These two populations of neurons are selected for representing the leftward or rightward directions of movements. **Figure 3b** shows the motion of the dots. Notice that most dots move in one direction under high motion coherence. When motion coherence is low, there is no directional preference or bias. **Figure 3c** shows the trade-offs among speed, accuracy, and cost where an optimum seems to emerge.

When the input threshold dominates the regulation (at the upper bound of the input), the total cost increases as the accuracy increases and decreases as the decision time decreases (105). When the amount of stimulus input to the system becomes the dominant mechanism, the total cost in decision making changes nonmonotonically when the additional input increases (105). Suboptimal accuracy and performance can be realized with optimal energy cost and speed (105) (see **Figure 3**). For decision making, then, such a system can operate at maximum speed and intermediate accuracy for a minimal energy cost. Therefore, in the neural decision-making process, both the landscape and flux are driving forces for the dynamics (speed, path, and accuracy) and thermodynamics.

This helps us to quantify the relations among speed, accuracy, and energy cost and to uncover the underlying mechanisms of decision making.

2.6. Energy Cost for Fidelity, Specificity, Cooperativity, and Sensitivity in Biosynthesis, Cell Signaling, and Immunity

Nonequilibrium thermodynamic cost can significantly influence the fidelity of biosynthesis. This can occur through a so-called kinetic proofreading mechanism for error correction (44, 65), which leads to the discrimination between the reaction pathway to the correct product and the reaction pathways to incorrect products. The probability of the correct product (fidelity) becomes significantly higher than the probability that one would estimate purely from the difference in the activation energies between the correct and incorrect reaction pathways (44, 65). The proofreading mechanism relies on the presence of an irreversible reaction step that leaves the reaction pathway. The irreversible step increases the probability of intermediates leaving the pathway toward the incorrect products, compared to the probability of leaving the pathway toward correct products. The fidelity of the reaction to the correct product can be increased by increasing the ratio between the two rate constants of leaving the pathways. This process can be repeated to further increase the fidelity. The irreversible reaction step in this case explicitly breaks the time reversal symmetry and therefore the detailed balance. It is the origin of the deviation from equilibrium. The irreversible reaction step is supported by the thermodynamic cost through the ATP consumption. It was quantitatively demonstrated that higher thermodynamic cost leads to higher fidelity (44, 65).

The kinetic proofreading mechanism is important not only for biosynthesis, but also for enzymatic reactions, for example, in cell signaling. In this case, the binding affinities are determined by the structures and interactions of the biomolecules (for example, kinases and their substrate proteins). In addition, the biomolecules are often required to bind with great specificity: A signaling molecule must bind specifically to the right partner to propagate a signal cascade. The specificity required for discriminating binding partners is usually based on the molecular structure and the associated interactions (55, 93, 107). However, a structural and thermodynamic approach to specificity often cannot meet the high requirements of the biological functions. Kinetic proofreading can help to resolve this issue beyond the structures and thermodynamics. It can increase the specificity by introducing nonequilibrium irreversible kinetic steps. This effectively enlarges the affinity difference between correct and incorrect targets and increases the ratio of the specific binding affinity to the nonspecific affinity (70–72). Again, the energy cost through phosphorylation or dephosphorylation via ATP hydrolysis is required to support the specificity discrimination.

High sensitivity is often important in cell signal transduction. This is often thought to be realized by the cooperativity of allosteric interactions. Such sensitivity requires a sufficient number of regulating proteins to be present: Enough materials must be supplied. However, high sensitivity can also be realized through kinetic cooperativity, which requires the presence of only a small number of regulatory proteins. The trade-off is that the kinetic cooperativity requires energy to be expended through ATP hydrolysis. High sensitivity can be realized by either allosteric cooperativity, with sufficient numbers of regulatory proteins present, or by kinetic cooperativity, with fewer regulators but sufficient energy expenditure (25, 31, 70–72). If there is a rich source of regulatory molecules, as in the environment of metabolites, then the allosteric cooperative interactions will be suitable for reaching the high sensitivity. However, if regulators are limited to only a small number, as in visual photon detection, then kinetic cooperativity is more suitable.

In immunity, T cells need to discriminate the molecules of the self from foreign intruders. The specificity of the receptor structure and binding affinity often is not sufficient for the

discrimination function of T cells. The kinetic proofreading mechanism of an irreversible kinetic step, supported by the energy cost from ATP hydrolysis, is again helpful in providing the specificity necessary for discrimination of the self from the nonself (32, 57).

2.7. Energy Cost in Cell Sensing

Cells can sense changes in the environment with high precision (9, 11, 18, 22, 27, 36, 90, 99). What is the fundamental limit of this precision? Cells sense chemical signals through receptors. The precision of sensing will be influenced by both the diffusive transport of the signaling molecules to the receptor and the binding to the receptor. Cells can increase the sensing precision by increasing the number of measurements (9), either by increasing the number of receptors or by increasing the number of measurements per receptor during certain integration times. The requirement for precision sets the receptor correlation time, the decay time scale of the fluctuations of the receptors. The downstream signaling pathways then integrate these receptor-state fluctuations from the upstream. The number of receptors, the receptor correlation time, and the effective integration time together contribute to the precision of sensing. It was shown that signaling networks integrate the receptor state nonuniformly in time so that cells can go beyond the well-known uniform integration Berg-Purcell limit by approximately a factor of ten (33).

It was shown that equilibrium signaling networks can achieve sensing. This implies that energy dissipation is not crucial for sensing (34). However, the associated sensing accuracy is limited by the number of receptors. This is due to the fact that equilibrium sensing displays a fundamental trade-off between the removal of extrinsic and of intrinsic noise (34). In nonequilibrium signaling systems, the burden of this trade-off can be lifted. This is realized by integrating the receptor state over time while suppressing the intrinsic noise through energy consumption for the purpose of storing the receptor state in stable chemical modification states of readout molecules (34, 35, 68). Thus, for nonequilibrium signaling systems, a combination of three resources is fundamentally required for sensing precision: receptors and their integration times, readout molecules, and energy cost. The combination of these three resources sets a fundamental sensing limit (7, 34, 35, 68). Thus, the sensing precision is limited by the combination of these three resources and will not be enhanced further by increasing another resource. Due to the architectural differences between cell signaling networks and computation, cellular sensing is unlikely to reach the well-known Landauer limit (67) of the optimal trade-off between accuracy and energy cost.

2.8. Thermodynamic Cost in Cell Adaptation

Sensory adaptation is a crucial regulatory function found in many living systems. The main function of the adaptation is to maintain sensitivity and fitness in changing environments. Many sensory adaptations are supported by underlying feedback networks in systems such as bacterial chemotaxis (40), osmotic sensing in yeast (42), and olfactory (58) and light sensing (61) in mammalian sensory neurons. This raises the questions of what supports the adaptation, and what the associated energy costs and feedback controls are. A core negative feedback control network commonly shared in various adaptation systems has been explored (51). It was shown that negative feedback control is out of equilibrium and supported by energy consumption (51). The energy expenditure is required to stabilize the adapted state against fluctuations. This leads to a quantitative relationship among the amount of sensory adaptation, its speed and accuracy, and its minimum energy cost. Direct measurements of the adaptation of starving *Escherichia coli* cells illustrated that adaptation slows down but maintains its accuracy (51, 90). These measurements support the speed–accuracy–energy cost trade-off for sensory adaptation (51).

DISCLOSURE STATEMENT

The authors are not aware of any affiliations, memberships, funding, or financial holdings that might be perceived as affecting the objectivity of this review.

AUTHOR CONTRIBUTIONS

X.F. wrote Sections 2.3, 2.4, 2.7, and 2.8.

ACKNOWLEDGMENTS

J.W. would like to thank the National Science Foundation (NSF) and National Institutes of Health (NIH) for support under grants NSF-PHY-76066, NSF-CHE-1808474, and NIH-R01GM124177.

LITERATURE CITED

1. Abbott L. 2008. Theoretical neuroscience rising. *Neuron* 60:489–95
2. Ackers GK, Johnson AD, Shea MA. 1982. Quantitative model for gene regulation by lambda phage repressor. *PNAS* 79:1129–33
3. Alberts B, Johnson A, Lewis J, Morgan D, Raff M, et al. 2015. *Molecular Biology of the Cell*. New York: Garland Sci. 6th ed.
4. Alex R, Anders L. 2008. Neurobiological models of two-choice decision making can be reduced to a one-dimensional nonlinear diffusion equation. *PLoS Comput. Biol.* 4:e1000046
5. Alon U. 2007. *An Introduction to Systems Biology*. London: Chapman & Hall
6. Artyomov MN, Das J, Kardar M, Chakraborty A. 2007. Purely stochastic binary decisions in cell signaling models without underlying deterministic bistabilities. *PNAS* 104:18958–63
7. Becker NB, Mugler A, ten Wolde PR. 2015. Optimal prediction by cellular signaling networks. *Phys. Rev. Lett.* 115:258103
8. Becskei A, Serrano L. 2000. Engineering stability in gene networks by autoregulation. *Nature* 405:590–93
9. Berg HC, Purcell EM. 1977. Physics of chemoreception. *Biophys. J.* 20:193–219
10. Bishop LM, Qian H. 2010. Stochastic bistability and bifurcation in a mesoscopic signaling system with autocatalytic kinase. *Biophys. J.* 98:1–11
11. Boeckh J, Kaissling KE, Schneider D. 1965. Insect olfactory receptors. *Cold Spring Harb. Symp. Quant. Biol.* 30:263–80
12. Chen KC, Calzone L, Csikasz-Nagy A, Cross FR, Novak B, Tyson JJ. 2004. Integrative analysis of cell cycle control in budding yeast. *Mol. Biol. Cell* 15:3841–62
13. Chen KC, Csikasz-Nagy A, Gyorfy B, Val J, Novak B, Tyson JJ. 2000. Kinetic analysis of a molecular model of the budding yeast cell cycle. *Mol. Biol. Cell* 11:369–91
14. Choi PJ, Long C, Kirsten F, Xie XS. 2008. A stochastic single-molecule event triggers phenotype switching of a bacterial cell. *Science* 322:442–46
15. Churchland AK, Roozbeh K, Shadlen MN. 2008. Decision-making with multiple alternatives. *Nat. Neurosci.* 11:693–702
16. Claude G, Albert G. 2009. Temporal self-organization of the cyclin/Cdk network driving the mammalian cell cycle. *PNAS* 106:21643–48
17. Davidson E. 2001. *Genomic Regulatory Systems: Development and Evolution*. Amsterdam: Elsevier
18. Dubuis JO, Tkačik G, Wieschaus EF, Gregor T, Bialek W. 2013. Positional information, in bits. *PNAS* 110:16301–8
19. Edman L, Földes-Papp Z, Wennmalm S, Rigler R. 1999. The fluctuating enzyme: a single molecule approach. *Chem. Phys.* 247:11–22
20. Edman L, Rigler R. 2000. Memory landscapes of single-enzyme molecules. *PNAS* 97:8266–71

21. English BP, Min W, van Oijen AM, Lee KT, Luo G, et al. 2006. Ever-fluctuating single enzyme molecules: Michaelis-Menten equation revisited. *Nat. Chem. Biol.* 2:87–94
22. Erdmann T, Howard M, ten Wolde PR. 2009. Role of spatial averaging in the precision of gene expression patterns. *Phys. Rev. Lett.* 103:258101
23. Feng H, Han B, Wang J. 2011. Adiabatic and non-adiabatic non-equilibrium stochastic dynamics of single regulating genes. *J. Phys. Chem. B* 115:1254–61
24. Feng H, Wang J. 2011. Potential and flux decomposition for dynamical systems and non-equilibrium thermodynamics: curvature, gauge field, and generalized fluctuation-dissipation theorem. *J. Chem. Phys.* 135:234511
25. Ferrell J, Xiong W. 2001. Bistability in cell signaling: how to make continuous processes discontinuous, and reversible processes irreversible. *Chaos* 11:227–36
26. Gardiner C. 2004. *Handbook of Stochastic Methods: For Physics, Chemistry and the Natural Sciences*. Berlin: Springer. 3rd ed.
27. Gasper T, Thomas G, William B. 2008. The role of input noise in transcriptional regulation. *PLOS ONE* 3:e2774
28. Gérard C, Goldbeter A. 2010. From simple to complex patterns of oscillatory behavior in a model for the mammalian cell cycle containing multiple oscillatory circuits. *Chaos* 20:045109
29. Gérard C, Goldbeter A. 2012. Entrainment of the mammalian cell cycle by the circadian clock: modeling two coupled cellular rhythms. *PLOS Comput. Biol.* 8:e1002516
30. Gold JI, Shadlen MN. 2007. The neural basis of decision making. *Annu. Rev. Neurosci.* 30:535–74
31. Goldbeter A, Koshland D. 1981. An amplified sensitivity arising from covalent modification in biological systems. *PNAS* 78:6841–44
32. Goldstein B, Faeder J, Hlavacek W. 2004. Mathematical and computational models of immune-receptor signalling. *Nat. Rev. Immunol.* 4:445–56
33. Govern CC, ten Wolde PR. 2012. Fundamental limits on sensing chemical concentrations with linear biochemical networks. *Phys. Rev. Lett.* 109:218103
34. Govern CC, ten Wolde PR. 2014. Energy dissipation and noise correlations in biochemical sensing. *Phys. Rev. Lett.* 113:258102
35. Govern CC, ten Wolde PR. 2014. Optimal resource allocation in cellular sensing systems. *PNAS* 111:17486–91
36. Gregor T, Tank DW, Wieschaus EF, Bialek W. 2007. Probing the limits to positional information. *Cell* 130:153–64
37. Haken H. 1987. *Advanced Synergetics: Instability Hierarchies of Self-Organizing Systems and Devices*. Berlin: Springer
38. Han B, Wang J. 2007. Quantifying robustness and dissipation cost of yeast cell cycle network: the funneled energy landscape perspectives. *Biophys. J.* 92:3755–63
39. Hassler K, Rigler P, Blom H, Rigler R, Widengren J, Lasser T. 2007. Dynamic disorder in horseradish peroxidase observed with total internal reflection fluorescence correlation spectroscopy. *Opt. Express* 15:5366–75
40. Hazelbauer GL, Falke JJ, Parkinson JS. 2008. Bacterial chemoreceptors: high-performance signaling in networked arrays. *Trends Biochem. Sci.* 33:9–19
41. Hejmadi M. 2009. *Introduction to Cancer Biology*. London: Bookboon
42. Hohmann S. 2002. Osmotic stress signaling and osmoadaptation in yeasts. *Microbiol. Mol. Biol. Rev.* 66:300–72
43. Hong Q, Elson EL. 2002. Single-molecule enzymology: stochastic Michaelis-Menten kinetics. *Biophys. Chem.* 101:565–76
44. Hopfield J. 1974. Kinetic proofreading: a new mechanism for reducing errors in biosynthetic processes requiring high specificity. *PNAS* 71:4135–39
45. Hopfield JJ. 1982. Neural networks and physical systems with emergent collective computational abilities. *PNAS* 79:2554–58
46. Hornos J, Schultz D, Innocentini G, Wang J, Walczak A, et al. 2005. Self-regulating gene: an exact solution. *Phys. Rev. E* 72:051907

47. Jackson EA. 1989. *Perspectives of Nonlinear Dynamics*. Cambridge, UK: Cambridge Univ. Press
48. Jiang Z, Tian L, Fang X, Zhang K, Liu Q, et al. 2019. The emergence of the two cell fates and their associated switching for a negative auto-regulating gene. *BMC Biol.* 17(1):49
49. Jianshu C. 2011. Michaelis-Menten equation and detailed balance in enzymatic networks. *J. Phys. Chem. B* 115:5493–98
50. Kepler TB, Elston TC. 2001. Stochasticity in transcriptional regulation: origins, consequences, and mathematical representations. *Biophys. J.* 81:3116–36
51. Lan G, Sartori P, Neumann S, Sourjik V, Tu Y. 2012. The energy-speed-accuracy trade-off in sensory adaptation. *Nat. Phys.* 8:422–28
52. Li C, Wang J. 2014. Landscape and flux reveal a new global view and physical quantification of mammalian cell cycle. *PNAS* 111:14130–35
53. Li Z, Hertz J. 2000. Odour recognition and segmentation by a model olfactory bulb and cortex. *Network* 11:83–102
54. Liu Q, Wang J. 2020. Quantifying the flux as the driving force for nonequilibrium dynamics and thermodynamics in non-Michaelis-Menten enzyme kinetics. *PNAS* 117(2):923–30
55. Lu Q, Lu PH, Wang J. 2007. Exploring the mechanism of flexible biomolecular recognition with single molecule dynamics. *Phys. Rev. Lett.* 98:128105
56. Luo X, Xu L, Han B, Wang J. 2017. Funneled potential and flux landscapes dictate the stabilities of both the states and the flow: fission yeast cell cycle. *PLOS Comput. Biol.* 13:e1005710
57. McKeithan T. 1995. Kinetic proofreading in T-cell receptor signal transduction. *PNAS* 92:5042–46
58. Menini A. 1999. Calcium signalling and regulation in olfactory neurons. *Curr. Opin. Neurobiol.* 9:419–26
59. Moerner WE, Fromm DP. 2003. Methods of single-molecule fluorescence spectroscopy and microscopy. *Rev. Sci. Instrum.* 74:3597–619
60. Mohr PN, Biele G, Heekeren HR. 2010. Neural processing of risk. *J. Neurosci.* 30:6613–19
61. Nakatani K, Tamura T, Yau KW. 1991. Light adaptation in retinal rods of the rabbit and two other nonprimate mammals. *J. Gen. Physiol.* 97:413–35
62. Nelson JM, Vosburgh WC. 1927. Kinetics of invertase action. *J. Am. Chem. Soc.* 13:223–36
63. Nicolis G. 1986. Dissipative systems. *Rep. Prog. Phys.* 49:873–949
64. Nicolis G, Prigogine I. 1977. *Self-Organization in Nonequilibrium Systems: From Dissipative Structures to Order Through Fluctuations*. New York: Wiley
65. Ninio J. 1975. Kinetic amplification of enzyme discrimination. *Biochimie* 57:587–95
66. Niwa M, Ditterich J. 2008. Perceptual decisions between multiple directions of visual motion. *J. Neurosci.* 28:4435–45
67. Ouldrige TE, Govern CC, ten Wolde PR. 2017. The thermodynamics of computational copying in biochemical systems. *Phys. Rev. X* 7:021004
68. Pankaj M, Schwab DJ. 2012. Energetic costs of cellular computation. *PNAS* 109:17978–82
69. Qi H, Blanchard A, Lu T. 2013. Engineered genetic information processing circuits. *Wiley Interdiscip. Rev. Syst. Biol. Med.* 5:273–87
70. Qian H. 2003. Thermodynamic and kinetic analysis of sensitivity amplification in biological signal transduction. *Biophys. Chem.* 105:585–93
71. Qian H. 2007. Phosphorylation energy hypothesis: open chemical systems and their biological functions. *Annu. Rev. Phys. Chem.* 58:113–42
72. Qian H. 2008. Cooperativity and specificity in enzyme kinetics: a single-molecule time-based perspective. *Biophys. J.* 95:10–17
73. Qian H. 2009. Entropy demystified: the “thermo”-dynamics of stochastically fluctuating systems. *Methods Enzymol.* 467:111–34
74. Qian MP, Qian M. 1979. Decomposition into a detailed balance part and a circulation part of an irreversible stationary Markov chain. *Sci. Sin. Special Issue II*:69–79
75. Ratcliff R, Rouder JN. 2010. Modeling response times for two-choice decisions. *Psychol. Sci.* 9:347–56
76. Ratcliff R, Zandt TV, McKoon G. 1999. Connectionist and diffusion models of reaction time. *Psychol. Rev.* 106:261–300
77. Reichl LE. 2009. *A Modern Course in Statistical Physics*. New York: Wiley. 3rd ed.

78. Sagawa T. 2013. *Thermodynamics of Information Processing in Small Systems*. Berlin: Springer
79. Schnakenberg J. 1976. Network theory of microscopic and macroscopic behavior of master equation systems. *Rev. Mod. Phys.* 48:571–85
80. Schultz D, Onuchic J, Wolynes P. 2007. Understanding stochastic simulations of the smallest genetic networks. *J. Chem. Phys.* 126:245102
81. Seifert U. 2008. Stochastic thermodynamics: principles and perspectives. *Eur. Phys. J. B* 64:423–31
82. Shadlen MN, Newsome WT. 2001. Neural basis of a perceptual decision in the parietal cortex (area LIP) of the rhesus monkey. *J. Neurophysiol.* 86:1916–36
83. Singh A, Weinberger LS. 2009. Stochastic gene expression as a molecular switch for viral latency. *Curr. Opin. Microbiol.* 12:460–66
84. Swain P, Elowitz M, Siggia E. 2002. Intrinsic and extrinsic contributions to stochasticity in gene expression. *PNAS* 99:12795–800
85. Tyson JJ, Bela N. 2008. Temporal organization of the cell cycle. *Curr. Biol.* 18:R759–68
86. Tyson JJ, Novak B. 2001. Regulation of the eukaryotic cell cycle: molecular antagonism, hysteresis, and irreversible transitions. *J. Theor. Biol.* 210:249–63
87. Van den Broeck C, Esposito M. 2010. Three faces of the second law. II. Fokker-Planck formulation. *Phys. Rev. E* 82:011144
88. Van Kampen N. 2007. *Stochastic Processes in Physics and Chemistry*. Amsterdam: Elsevier
89. Vellela M, Qian H. 2010. On the Poincaré-Hill cycle map of rotational random walk: locating the stochastic limit cycle in a reversible Schnakenberg model. *Proc. Math. Phys. Eng. Sci.* 466:771–88
90. Victor S, Berg HC. 2002. Receptor sensitivity in bacterial chemotaxis. *PNAS* 99:123–27
91. Vogels T, Rajan K, Abbott L. 2005. Neural network dynamics. *Annu. Rev. Neurosci.* 28:357–76
92. Wang J. 2015. Landscape and flux theory of non-equilibrium dynamical systems with application to biology. *Adv. Phys.* 64:1–137
93. Wang J, Verkhivker GM. 2003. Energy landscape theory, funnels, specificity and optimal criterion of biomolecular binding. *Phys. Rev. Lett.* 90:188101
94. Wang J, Xu L, Wang E. 2008. Potential landscape and flux framework of nonequilibrium networks: robustness, dissipation, and coherence of biochemical oscillations. *PNAS* 105:12271–76
95. Wang J, Zhang K, Wang E. 2010. Kinetic paths, time scale, and underlying landscapes: a path integral framework to study global natures of nonequilibrium systems and networks. *J. Chem. Phys.* 133:125103
96. Wang XJ. 2002. Probabilistic decision making by slow reverberation in cortical circuits. *Neuron* 36:955–68
97. Wang XJ. 2008. Decision making in recurrent neuronal circuits. *Neuron* 60:215–34
98. Wei M, Gopich IV, English BP, Kou SC, Xie XS, Szabo A. 2006. When does the Michaelis-Menten equation hold for fluctuating enzymes? *J. Phys. Chem. B* 110:20093–97
99. William B, Sima S. 2005. Physical limits to biochemical signaling. *PNAS* 102:10040–45
100. Wong K, Huk A, Shadlen M, Wang X. 2007. Neural circuit dynamics underlying accumulation of time-varying evidence during perceptual decision making. *Front. Comput. Neurosci.* 1:6
101. Wong K, Wang X. 2006. A recurrent network mechanism of time integration in perceptual decisions. *J. Neurosci.* 26:1314–28
102. Xu L, Shi H, Feng H, Wang J. 2012. The energy pump and the origin of the non-equilibrium flux of the dynamical systems and the networks. *J. Chem. Phys.* 136:165102
103. Yan H, Li B, Wang J. 2019. Non-equilibrium landscape and flux reveal how the central amygdala circuit gates passive and active defensive responses. *J. R. Soc. Interface* 16:20180756
104. Yan H, Wang J. 2017. Quantification of motor network dynamics in Parkinson's disease by means of landscape and flux theory. *PLOS ONE* 12:e0174364
105. Yan H, Zhang K, Wang J. 2016. Physical mechanism of mind changes and tradeoffs among speed, accuracy, and energy cost in brain decision making: landscape, flux, and path perspectives. *Chin. Phys. B* 25:078702
106. Yan H, Zhao L, Hu L, Wang X, Wang E, Wang J. 2013. Nonequilibrium landscape theory of neural networks. *PNAS* 110:E4185–94

107. Yan Z, Zheng X, Wang E, Wang J. 2013. Thermodynamic and kinetic specificities of ligand binding. *Chem. Sci.* 4:2387–95
108. Zhang F, Xu L, Zhang K, Wang E, Wang J. 2012. The potential and flux landscape theory of evolution. *J. Chem. Phys.* 137:065102
109. Zhang K, Wang J. 2018. Exploring the underlying mechanisms of the *Xenopus laevis* embryonic cell cycle. *J. Phys. Chem. B* 122:5487–99
110. Zhang Z, Wang J. 2014. Curl flux, coherence, and population landscape of molecular systems: nonequilibrium quantum steady state, energy (charge) transport, and thermodynamics. *J. Chem. Phys.* 140:245101
111. Zhang Z, Wang J. 2015. Landscape, kinetics, paths and statistics of curl flux, coherence, entanglement and energy transfer in non-equilibrium quantum systems. *New J. Phys.* 17:043053